Experimental modal identification of smart composite structure applied to active vibration control

Jonathan Rodriguez, Manuel Collet, Simon Chesné

Experimental modal identification of smart composite structure applied to active vibration control

Jonathan Rodriguez[1,*], **Manuel Collet**[2] and **Simon Chesné**[1]

[1] Université de Lyon, CNRS INSA-Lyon, LaMCoS UMR5229, Villeurbanne F-69621, France
[2] Université de Lyon, Ecole Centrale de Lyon, ENISE, ENTPE, CNRS, Laboratoire de Tribologie et Dynamique des Systèmes LTDS UMR5513, F-69134 Ecully, France

E-mail: jonathan.rodriguez@insa-lyon.fr

Abstract

This paper proposes an experimental modal identification method for vibration control of multi-actuators and multi-sensors complex smart structures. The general formulation avoids the difficulty of the coupling coefficients identification in electromechanical systems through a modal reduced-order model and uses first-order polynomials as phase correctors for the numerators of the identified transfer functions. Then, a frequency-shaped linear quadratic controller is designed to control multiple modes on a smart composite structure with integrated transducers. The experimental results obtained in terms of multi-modal vibration control were promising with attenuations up to 20 dB on the target modes, confirming the efficiency of the proposed identification and control method for future applications with more extended and complex composite smart structures.

Keywords: vibration control, active modal control, piezoelectric transducers, smart composite structures

1. Introduction

Composite smart structures demonstrated in the last years a great potential in many applications. By integrating piezoelectric (PZT) transducers directly into the composite layers or even simply bonding them to the external layer, voltages can be measured or applied as images of the strain experienced by the structure or the stress applied by the transducers themselves as actuators.

These integrated hybrid structures present two main advantages compared to more traditionally actuated systems using electric motors or voice-coil actuators. The first one being lighter, as the actuation does not include permanent magnets. And secondly, the actuators can be more easily distributed over complex curved structural surfaces in network configurations. This last point provides a better distribution of the actuation on the structure and can improve the control authority of the transducers onto it or the observability of the dynamic strain.

Thus, the field of applications of such structures are mainly structural health monitoring [1], active vibration control [2] and energy harvesting [3].

Now focusing on composite smart structures for active vibration control, the challenge of such systems is in the design of robust and efficient controllers, whether the objective is broadband vibration control, disturbance rejection, or modal control. Performance is in general based on a first step which is precise modeling of the considered dynamic system with the characterization of all the interactions between each PZT actuator and sensor.

Naturally, the first approach has been to design controllers based on analytical models of simple and well-defined structures such as composite cantilever beams [4–6] or plates [7]

* Author to whom any correspondence should be addressed.

with bonded or integrated PZT transducers [8] to reduce the dispersion between the model and the actual system. For these structures, the identification stage is reduced to its minimum thanks to well-controlled parameters such as geometry, material properties, and easily determined electromechanical coupling coefficients.

However, accurate analytical modeling of coupled electromechanical systems becomes quickly complex with real industrial structures, typically curved shapes. Many research has been carried out using finite-elements (FEs) models of the considered structures to feed observers and controllers [9–11]. Li F.-M *et al* proposed in [12] an analytical approach to derive the equations of motion of a conical shell and control its vibrations using PZT patches with LQR control method. Even considering a homogenous, isotropic, and thin material, the model remains difficult to set up and yet no correlation has been shown with experimental results.

Besides the complexity of modeling the physical behavior of curved surfaces with bonded PZT transducers, accurate characterization of the electromechanical coupling factors in real smart structures is also a challenge in itself due to high dispersion level [13], especially in weakly coupled systems.

When it comes to active modal control of complex smart structures, the identification stage can be simplified from an analytical or FE model approach as mentioned earlier to a curve-fitting problem where the frequency response functions (FRFs) of the PZT sensors to the actuators are considered as sums of n modal responses, described with 2nd order rational transfer functions. The modal parameters such as frequency and damping ratio are then estimated for each observed/controlled mode from the FRF and implemented into a state-space realization of the system [14, 15].

Besides, as collocated actuators/sensors are not always an option, a phase correction is in general necessary for the modal transfer function approximation to fit with the experimental FRF at the frequency of each mode. In [16], the state matrix A of the state-space realization is filled with the experimentally identified modal parameters while the actuation and observation matrices B and C respectively still contain the theoretical electromechanical coupling factors with the possible dispersion mentioned earlier for complex, curved shaped composite structures. A common solution to deal with non-collocated control is to correct the modal phase with suitable time delays within the closed-loop such as in [17, 18]. Qiu Z proposed also in [19] to introduce an identified time delay to correct the phase from the theoretical modal model obtained by FE method, controlling the first three bending modes and two torsional modes of a composite plate. However, introducing time delays in closed-loop systems is not always desirable since they can, if not handled properly, lead to instability, also making the closed-loop nonlinear.

All these studies on composite smart structures active vibration control highlight the difficulty, when facing complex structures, to obtain a precise model. Thus, curved shapes, non-homogeneous materials and non-linear damping cause indeed high modeling uncertainties, degrading the performance of any analytical-based controller. To tackle such difficulty, experimental approaches describing the structure behavior using modal superimposition simplify this stage providing a sufficiently precise estimation of the experimental FRF at the frequencies of the observed and controlled modes. This problem is the main motivation for this work. Yet, the phase correction needed for non-collocated control has to be implemented into the state-space realization of the system.

The contribution of this paper is to propose a general state-space formulation, oriented toward active multi-modal control, for complex smart structures with multiple actuators and sensors. No theoretical model of the electromechanical coupled system is needed and the modal parameters of the desired controlled modes are obtained by curve fitting from the experimental FRF's. The novelty lies especially into the modal phase correction formulation due to non-collocated control and nonlinear damping effects in the composite materials using suitable 1st order polynomials at the numerator of the modal response rational functions. No time delays are used within the closed-loop which remains linear. In addition, the controlled smart composite structure used for the experiments is curved shaped and the PZT transducers are directly integrated between the fiber layers.

This paper is organized as follows. The next section 2 contains the contribution and presents the development of the proposed modal state-space realization of the composite smart structure. Then, the frequency-shaped LQG controller is defined in section 3 and applied to the proposed state-space system. Finally, in section 4 are presented all the results of the modal identification method, the numerical parameters of the controller, and the experimental results.

2. System identification

Let us consider a complex modal smart structure with N_a PZT actuators and N_s PZT sensors. In the modeling process, n structure vibration modes are chosen to be observed and controlled, within the desired bandwidth, and sufficiently separated to consider that at the characteristic frequency of the ith mode ω_i, the contribution of the mode $j \neq i$ is negligible.

Thus, the transfer function $H_{k,l}(s)$ $[V/V]$ between actuator l voltage input and sensor k voltage output can be approximated by the sum of n modal responses:

$$H_{k,l}(s) = \sum_{i}^{n} \frac{M_i^{k,l} e^{j\phi_i^{k,l}}}{s^2 + 2\xi_i\omega_i s + \omega_i^2} \tag{1}$$

where $s = j\omega$ is the Laplace variable, ω_i is the modal frequency and ξ_i the modal damping ratio. $M_i^{k,l}$ and $\phi_i^{k,l}$ are the modal magnitude and phase respectively of the ith mode. All these modal parameters can be estimated using the rational fraction form method (RFP) [20, 21] from the measured transfer function $H_{k,l}^{exp}(\omega)$.

The complex numerator in (1) is necessary here since the physical controlled system is a complex composite structure. Hence, the particular non-homogeneous material of the structure can show nonlinear, in addition to non-diagonalizable damping effects and also high modal superimposition causing such complex numerators in the transfer functions to arise.

A state-space formulation of subsystem G_l is now defined to characterize the transfer function vector between the PZT voltage input of the lth actuator $u_l \in \mathbb{R}$ and the PZT voltage response $y_l \in \mathbb{R}^{N_s}$ of the sensors in open circuit due to actuation signal u_l:

$$G_l \begin{cases} \dot{x}_l = A_l x_l + B_l u_l \\ y_l = C_l x_l + D_l u_l \end{cases} \tag{2}$$

with $A_l \in \mathbb{R}^{2n\times 2n}$, $B_l \in \mathbb{R}^{2n}$, $C_l \in \mathbb{R}^{N_s\times 2n}$, $D_l \in \mathbb{R}^{N_s}$, $x_l = [q_l, \dot{q}_l]^T$, $q_l \in \mathbb{R}^n$ and $\dot{q}_l \in \mathbb{R}^n$ being the modal state and its time derivative respectively. Let us recall that the matrices A_l, B_l, C_l and D_l correspond to the state, actuation, observation and feed-through matrices respectively. Since there is no feed-through in the considered system we have $D_l = 0_{Ns,1}$.

From (1) and (2), the matrices A_l, B_l and C_l can be written in the following intuitive form:

$$\begin{aligned} A_l &= \begin{bmatrix} 0_n & I_n \\ -\mathrm{diag}(\omega_i^2) & -2\mathrm{diag}(\xi_i\omega_i) \end{bmatrix}_{2n,2n} \\ B_l &= \begin{bmatrix} 0_{n,1} \\ B_1^l \\ \vdots \\ B_n^l \end{bmatrix}_{2n,N_a} \\ C_l &= \begin{bmatrix} C_1^1 & \cdots & C_n^1 & 0_{1,n} \\ \vdots & \ddots & \vdots & 0_{1,n} \\ C_1^{N_s} & \cdots & C_n^{N_s} & 0_{1,n} \end{bmatrix}_{N_s,2n} \end{aligned} \tag{3}$$

where I_n represents an identity matrix of dimension $n \times n$. The transfer function vector $G_l(s) \in \mathbb{C}^{N_s}$ of system (2) such that $Y_l(s) = G_l(s)U_l(s)$ is defined by:

$$G_l(s) = C_l\left(sI_{2n} - A_l\right)^{-1} B_l. \tag{4}$$

From (1) and (4), it comes the following identification between the state-space subsystem G_l and the rational form formulation $H_{k,l}(s)$:

$$M_i^{k,l} e^{j\phi_i^{k,l}} = C_i^k B_i^l. \tag{5}$$

In practice, the independent identification of the coefficients C_i^k and B_i^l from a generalized electromechanical model can be difficult, especially when coupling is weak since the precision drops down. Besides, only the products $C_i^k B_i^l$ are necessary to design the controller, the need for a more complex identification process to compute separately the coefficients C_i^k and B_i^l can be avoided. From this statement come the following suitable definitions for the matrices B_l and C_l where a choice is made to impose unit values to the coefficients B_i^l:

$$\begin{aligned} B_l &= [0_{1,n}\ 1_{1,n}]^T \\ C_l &= \begin{bmatrix} M_1^{1,l} e^{j\phi_1^{1,l}} & \cdots & M_n^{1,l} e^{j\phi_n^{1,l}} & 0_{1\times n} \\ \vdots & \ddots & \vdots & \vdots \\ M_1^{N_s,l} e^{j\phi_1^{N_s,l}} & \cdots & M_n^{N_s,l} e^{j\phi_n^{N_s,l}} & 0_{1\times n} \end{bmatrix}. \end{aligned} \tag{6}$$

Nevertheless, complex state-space systems ($C \in \mathbb{C}^{Ns\times 2n}$) are not desirable formulations for real-time experiments. In [22], this difficulty had been bypassed by replacing the coefficients $M_i^{k,l} e^{j\phi_i^{k,l}}$ with appropriate time delays, only keeping the amplitudes $M_i^{k,l}$ within the observation matrix C. Nevertheless, with structures to control getting more complex with multiple-modes, actuators and sensors, the use multiple delays in the closed-loop becomes quickly inconvenient.

The contribution of this paper is now the following step. With the objective to improve the identified state-space formulation (3) and (6), the next modification is proposed for (1) to fit with a regular polynomial rational transfer function:

$$H_{k,l}^{ident}(s) = \sum_i^n \frac{a_i^{k,l} + b_i^{k,l} s}{s^2 + 2\xi_i\omega_i s + \omega_i^2} \tag{7}$$

where $(a_i^{k,l}, b_i^{k,l}) \in \mathbb{R}^2$ and:

$$\begin{aligned} a_i^{k,l} &= Re(M_i^{k,l} e^{j\phi_i^{k,l}}) \\ b_i^{k,l} &= Im(M_i^{k,l} e^{j\phi_i^{k,l}}) \frac{1}{\omega_i}. \end{aligned} \tag{8}$$

Thus, the new transfer function (7) displays the correct magnitude and phase for each mode i as in (1). Finally, the observation matrix C_l is re-written as:

$$C_l = \begin{bmatrix} a_1^{1,l} & \cdots & a_n^{1,l} & b_1^{1,l} & \cdots & b_n^{1,l} \\ \vdots & \ddots & \vdots & \vdots & \ddots & \vdots \\ a_1^{N_s,l} & \cdots & a_n^{N_s,l} & b_1^{N_s,l} & \cdots & b_n^{N_s,l} \end{bmatrix} \tag{9}$$

providing the system (2) with all real matrices A_l, B_l and C_l. Now that the subsystems G_l are defined using a proper state-space formulation, the total system $G(s)$ summing the effects of each actuator such that

$$\begin{aligned} Y(s) &= \sum_{l=1}^{N_a} Y_l(s) \\ &= \sum_{l=1}^{N_a} G_l(s)U_l(s) \\ &= G(s)U(s) \end{aligned} \tag{10}$$

with $U(s) = [U_1(s)\ \ldots\ U_{Na}(s)]^T$. A state-space realization of G is:

$$G \begin{cases} \dot{x'} = A'x + B'u \\ y = C'x \end{cases} \tag{11}$$

where $x' = [x_1^T\ \ldots\ x_{Na}^T]^T$, $u = [u_1\ \ldots\ u_{Na}]^T$ and $y = \sum_{l=1}^{Na} y_l$. The matrices $A' \in \mathbb{R}^{2n.N_a\times 2n.N_a}$, $B' \in \mathbb{R}^{2n.N_a\times N_a}$, and $C' \in \mathbb{R}^{N_s\times 2n.N_a}$ have the following definition:

$$A' = \begin{bmatrix} A_1 & 0_{2n} & \cdots & 0_{2n} \\ 0_{2n} & A_2 & \cdots & 0_{2n} \\ \vdots & \vdots & \ddots & \vdots \\ 0_{2n} & 0_{2n} & \cdots & A_{N_a} \end{bmatrix}$$

$$B' = \begin{bmatrix} B_1 & 0_{2n,1} & \cdots & 0_{2n,1} \\ 0_{2n,1} & B_2 & \cdots & 0_{2n,1} \\ \vdots & \vdots & \ddots & 0_{2n,1} \\ 0_{2n,1} & 0_{2n,1} & \cdots & B_{N_a} \end{bmatrix}$$

$$C' = \begin{bmatrix} C_1 & C_2 & \cdots & C_{Na} \end{bmatrix}. \tag{12}$$

Nevertheless, this particular state-space realization is poorly balanced in terms of observability and controllability. The matrix B' is filled with unitary values while matrix C' contains the coefficients $a_i^{k,l}$ which are globally of the same order of magnitude than ω_i, making the system much more observable than controllable. Thus, using the Gramian method [23], a transformation matrix $T \in \mathbb{R}^{2n.N_a \times 2n.N_a}$ is computed such that the new state vector is $x = T^{-1}x'$. The new state-space realization of G is finally

$$G \begin{cases} \dot{x} = Ax + Bu \\ y = Cx \end{cases} \tag{13}$$

with $A = T^{-1}A'T$, $B = T^{-1}B'$ and $C = C'T$.

In conclusion, the proposed identification procedure is an improvement to the method presented in [22] since all the transfer functions between actuators and sensors are now completely defined in the state space system G, with no need for additional time delay correction. Thus, this formulation fits better to the dynamics of the real structure and also simplifies the design of a stable and robust control.

3. Control design

The controller is designed as a frequency-shaped linear quadratic regulator [24]. The objective is to focus the control energy on the identified modes from (1) and thereby minimize the following quadratic frequency dependent criterion:

$$J = \frac{1}{2}\int_{-\infty}^{+\infty} \left[x^*(j\omega)Q(j\omega)x(j\omega) + u^*(j\omega)R(j\omega)u(j\omega)\right] d\omega. \tag{14}$$

Thus, the functions $R^{-1/2}$ and $Q^{1/2}$ supposedly stable, respectively proper and strictly proper, are applied as pre- and post-filters to the original plant such as in figure 1. Their state-space realization are defined by:

$$R^{-1/2}(s) = \begin{cases} \dot{x}_R = A_R x_R + B_R \bar{u} \\ u = C_R x_R \end{cases} \tag{15}$$

$$Q^{1/2}(s) = \begin{cases} \dot{x}_Q = A_Q x_Q + B_Q y \\ \bar{y} = C_Q x_Q + D_Q y. \end{cases} \tag{16}$$

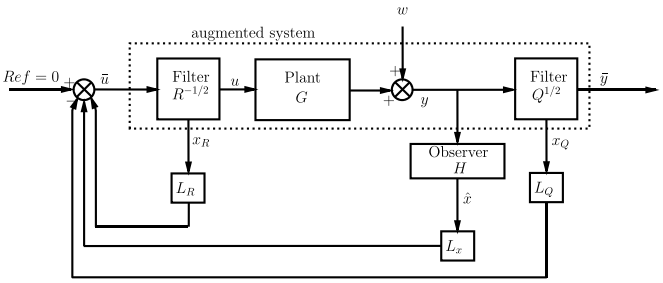

Figure 1. Closed-loop system with augmented plant and observer.

The augmented system with the new state vector $z = [x^T\ x_Q^T\ x_R^T]^T$ is now:

$$\begin{cases} [l]\begin{bmatrix} \dot{x} \\ \dot{x_Q} \\ \dot{x_R} \end{bmatrix} = \begin{bmatrix} A & 0 & BC_R \\ B_Q C & A_Q & 0 \\ 0 & 0 & A_R \end{bmatrix}\begin{bmatrix} x \\ x_Q \\ x_R \end{bmatrix} + \begin{bmatrix} 0 \\ 0 \\ B_R \end{bmatrix}\bar{u} \\ \bar{y} = [D_Q C\ C_Q\ 0]\begin{bmatrix} x \\ x_Q \\ x_R \end{bmatrix} \end{cases}$$

where $\bar{u} \in \mathbb{R}^{N_a}$ and $\bar{y} \in \mathbb{R}^{N_s}$ are the augmented system input and output. For the sake of simplicity, (17) is written as:

$$\begin{cases} \dot{z} = \tilde{A}z + \tilde{B}\bar{u} \\ \bar{y} = \tilde{C}z \end{cases}. \tag{17}$$

The gain matrix $\tilde{K} \in \mathbb{R}^{Na \times Ns}$ is now computed as solution to the LQR problem $(\tilde{A}, \tilde{B})$ such that:

$$\begin{aligned} \bar{u} &= -\tilde{K}z \\ &= -\tilde{K}_x x - \tilde{K}_Q x_Q - \tilde{K}_R x_R. \end{aligned} \tag{18}$$

Since the full-state feedback is necessary to compute the control signal $\bar{u}$, a Kalman observer is designed to estimate the state x from y such that:

$$\begin{cases} \dot{\hat{x}} = A\hat{x} + Bu + L(y - C\hat{x}) \\ \bar{u} = -\tilde{K}_x\hat{x} - \tilde{K}_Q x_Q - \tilde{K}_R x_R \end{cases} \tag{19}$$

where $\hat{x} \in \mathbb{R}^{2n}$ is the state estimation. The observer gain matrix L is designed considering low level of co-variance from measurement noise and expected state perturbation. Thus, the complete controller linking the measure y to the control signal u can be expressed as the following state-space system:

$$\begin{cases} [l]\begin{bmatrix} \dot{\hat{x}} \\ \dot{x_Q} \\ \dot{x_R} \end{bmatrix} = \begin{bmatrix} A - LC & 0 & BC_R \\ 0 & A_Q & 0 \\ -B_R\tilde{K}_x & -B_R\tilde{K}_Q & A_R - B_R\tilde{K}_R \end{bmatrix}\begin{bmatrix} \hat{x} \\ x_Q \\ x_R \end{bmatrix} \\ \qquad + \begin{bmatrix} L \\ B_Q \\ 0 \end{bmatrix} y \\ u = [0\ \ 0\ \ C_R]\begin{bmatrix} \hat{x} \\ x_Q \\ x_R \end{bmatrix} \end{cases}. \tag{20}$$

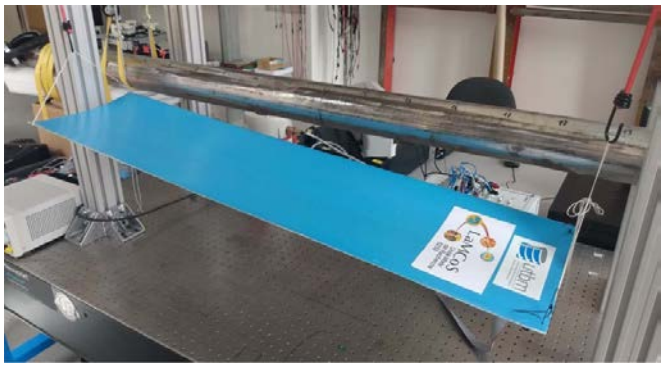

Figure 2. Smart composite structure: global view.

The transfer function matrix $K(s)$ of the controller is then obtained from straightforward calculation:

$$
\begin{aligned}
U(s) &= -K(s)Y(s) \\
K(s) &= C_R \left(B_R \tilde{K}_x (sI_{2n} - A + LC)^{-1} BC_R \right. \\
&\quad \left. + sI_R - A_R + B_R \tilde{K}_R \right)^{-1} B_R \left(\tilde{K}_x (sI_{2n} - A + LC)^{-1} L \right. \\
&\quad \left. + \tilde{K}_Q (sI_Q - A_Q)^{-1} B_Q \right)
\end{aligned}
$$

where I_R and I_Q are identity matrices of appropriate dimensions depending on the order of $R^{-1/2}(s)$ and $Q^{1/2}(s)$.

4. Experimentation on the composite smart structure

In this section, the experiments on the considered smart composite structure are presented, from the identification steps, to the controller tuning and finally the results of modal control.

4.1. Experimental setup

The experimental support is the composite smart structure presented in the figures 2 and 3 and was manufactured by the M3M Laboratory, UTBM-France. It is a spoiler type curved profile with a three layers structure: one active layer containing the considered six PZT transducers of 25 mm diameter and 150 μm thickness between two glass fiber layers. The transducers are all aligned and separated in the horizontal plane by 50 mm (center to center distance). The overall spoiler has the following dimensions: $1150 \times 300 \times 25$ mm.

A schematic representation of the physical system is given in figure 4 with the excitation, sensors, and actuators PZT transducers alongside the connections to the Dspace MicroLabBox controller and the computer. The composite smart structure is also suspended to the ground using low stiffness elastic components to isolate its dynamical response.

4.2. Identification results

Since a novel identification method is used in this approach, the two formulations (1) and (7) are now compared. A white noise signal of maximum amplitude 3 V and 20 s length is sent

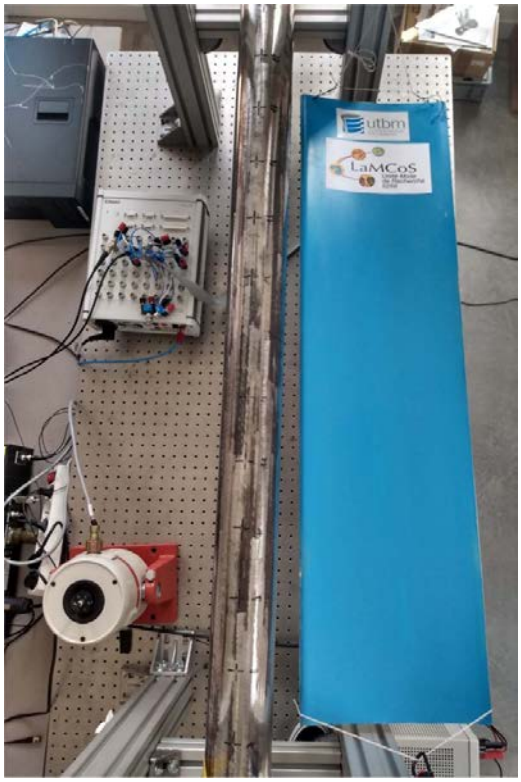

Figure 3. Smart composite structure: top view.

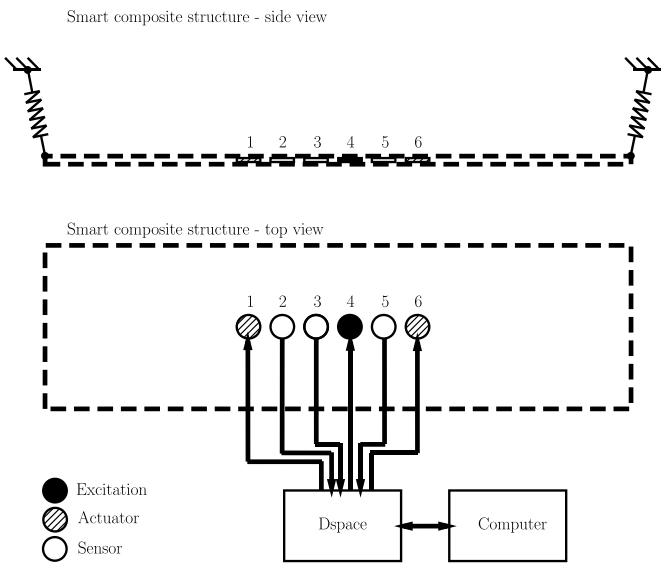

Figure 4. Schematic representation of the experiment.

to the PZT actuators 1 and 6 sequentially with a sample frequency of 20 kHz. All the measured FRF are displayed in the figures 5 and 6 where three target modes to be controlled are chosen: 770, 1282, and 1576 Hz. The choice of the bandwidth of interest between 500 and 2000 Hz is made regarding potential future acoustic applications. Besides, PZT transducers in general offer low control authority at low frequencies since their strain is very limited.

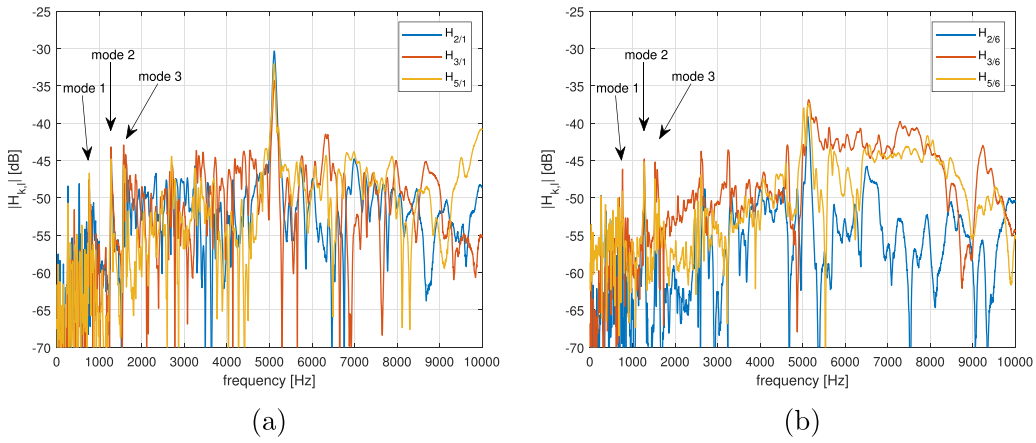

Figure 5. FRF's of PZT sensors 2, 3, and 5 to actuation (a) PZT 1 and (b) PZT 6, targeted modes for control.

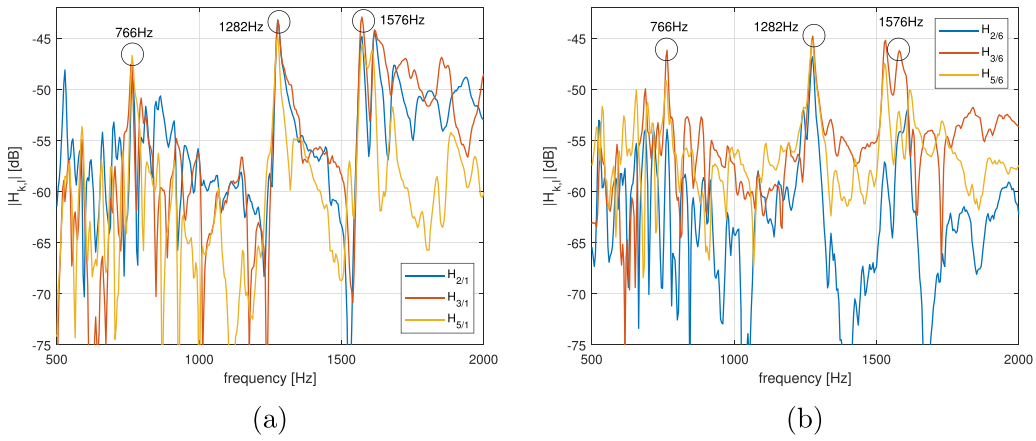

Figure 6. FRF's of PZT sensors 2, 3, and 5 to actuation (PZT 1 and 6), targeted modes for control with zoom on the bandwidth of interest.

Finally, the identified parameters are summarized in table 1. Since the identification results of the parameters ω_i and ξ_i are very close from one FRF to another, the reference modal parameters are arbitrarily taken from $H_{2,1}(s)$.

The measured FRF's from actuators to sensors and their respective reconstructions from expressions (7) and (7) are presented in the figures 7–9 for the transducers 2, 3, and 5 respectively.

One can easily observe that at the vicinity of the considered mode frequencies, the proposed identification procedure gives the correct magnitude and phase. However, as soon as the excitation frequency moves away from the modes, more and more deviation is visible between the measurements and the reconstructions. Yet, since the objective of the method is to focus the control energy on the target modes, these deviations do not interfere in the control loop in a way that performance is impacted drastically as it will be shown in section 4.4.

Last but not least, the proposed identification method provides both precision and easier algebraic formulation for state-space systems real-time experimentation compared to the solution in [22]. One can notice in figures 7–9 that both expressions (1) and (7) give similar results, if not identical around, the modes frequencies.

Remark. The figures 5–9 highlight the difficulty of identifying predominant modes in the PZT's voltage response. Thus, the measured FRF's frequency content is very complex and rich, increasing the challenge of identifying precisely the modal parameters. However, the results obtained in section 4.4 with the proposed control formulation demonstrate the robustness of the method with its ability to deal with parametric uncertainties, fused modes within noisy frequency measures, and weakly coupled electromechanical systems.

4.3. Control parameters

Finally, the weighting filters $Q^{1/2}$ and $R^{-1/2}$ are designed to emphasize the control effort on the target modes and remove lower and higher frequencies. $Q^{1/2}(s)$ is the product of a sum of modal filters around the target frequencies with a 2nd order high pass filter:

$$Q^{1/2}(s) = I_{N_s} \times k_Q \times \left(\frac{2\,\xi_f \omega_1^2}{s^2 + 2\,s\xi_f\omega_1^2 + \omega_1^2} + \frac{2\,\xi_f \omega_2^2}{s^2 + 2\,s\xi_f\omega_2^2 + \omega_2^2} + \frac{2\,\xi_f \omega_3^2}{s^2 + 2\,s\xi_f\omega_3^2 + \omega_3^2} \right) \times \frac{s^2/\omega_{HP}^2}{1 + s^2/\omega_{HP}^2 + s/(Q_f\omega_{HP})} \tag{21}$$

Table 1. Identified modal parameters from the three PZT sensors FRF's to actuation.

Mode	$\omega_i/(2\pi)$ (Hz)		ξ_i	
1	770		7.5×10^{-3}	
2	1282		5.0×10^{-3}	
3	1576		4.3×10^{-3}	
		$H_{2,1}$		
	Magnitude	Phase (deg)	$a_i^{2,1}$	$b_i^{2,1}$
1	1153	136	-0.827×10^3	0.1658
2	5484	140	-4.192×10^3	0.4389
3	5510	141	-4.269×10^3	0.3517
		$H_{2,6}$		
	Magnitude	Phase (deg)	$a_i^{2,6}$	$b_i^{2,6}$
1	847	-54	0.500×10^3	-0.1412
2	3634	-30	3.134×10^3	-0.2284
3	2214	-129	-1.395×10^3	-0.1736
		$H_{3,1}$		
	Magnitude	Phase (deg)	$a_i^{3,1}$	$b_i^{3,1}$
1	1965	-177	-1.961×10^3	-0.0237
2	5425	138	-4.020×10^3	0.4525
3	6763	138	-5.048×10^3	0.4546
		$H_{3,6}$		
	Magnitude	Phase (deg)	$a_i^{3,6}$	$b_i^{3,6}$
1	2115	-29	1.847×10^3	-0.2127
2	4789	-17	4.579×10^3	-0.1740
3	1179	-59	0.605×10^3	-0.1022
		$H_{5,1}$		
	Magnitude	Phase (deg)	$a_i^{5,1}$	$b_i^{5,1}$
1	1481	148	-1.253×10^3	0.1631
2	4640	155	-4.218×10^3	0.2398
3	4556	118	-2.130×10^3	0.4067
		$H_{5,6}$		
	Magnitude	Phase [deg]	$a_i^{5,6}$	$b_i^{5,6}$
1	1459	33	1.221×10^3	0.1649
2	4238	-20	3.990×10^3	-0.1774
3	1897	-75	0.495×10^3	-0.1849

where $k_Q = 2.10^5$, $\omega_{HP} = \omega_1$, $\xi_f = 7 \times 10^{-3}$, and $Q_f = 1$. This formulation for $Q^{1/2}$ allows to assign independent weighting coefficients to each mode and also easily implement supplementary modes in the control. $R^{-1/2}(s)$ is then designed as a 2nd order low pass filter:

$$R^{-1/2}(s) = I_{N_a} \times \frac{1}{1 + s^2/\omega_{LP}^2 + s/(Q_f \omega_{LP})} \tag{22}$$

where $\omega_{LP} = \omega_3$. The filters FRF's are displayed in figure 10. For the sake of practicality, the main control gain k_Q is arbitrarily set only within the filter $Q^{1/2}$, not in $R^{-1/2}$, and has been determined experimentally to avoid any instability of the closed-loop.

The designed LQG frequency-shaped controller is compared in the next subsection to classical LQG approach applied directly to the system G with the state space-realization (11) and an observer of the form (19) applied to (11). In this case,

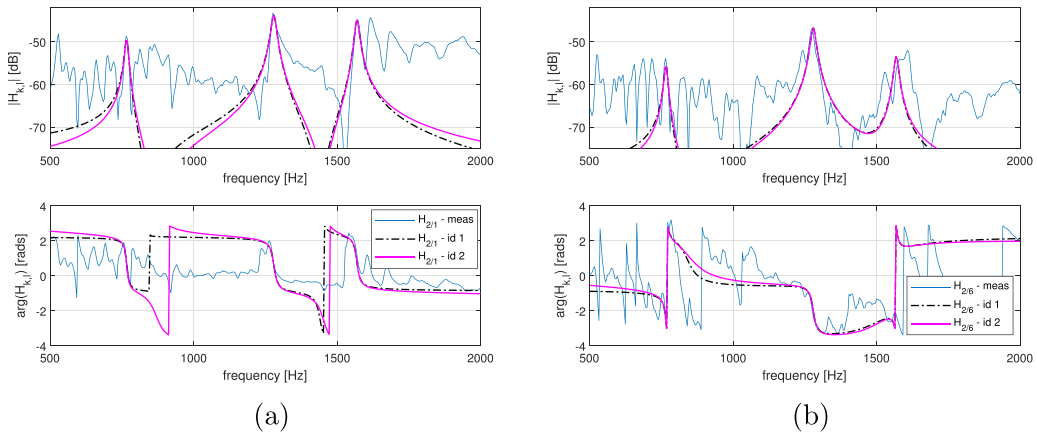

Figure 7. Identification : FRF's of PZT n°2 to actuation, (a) PZT 1 and (b) PZT 6, measurement, identification 1 with the formulation in (1), identification 2 with the proposed method in (7).

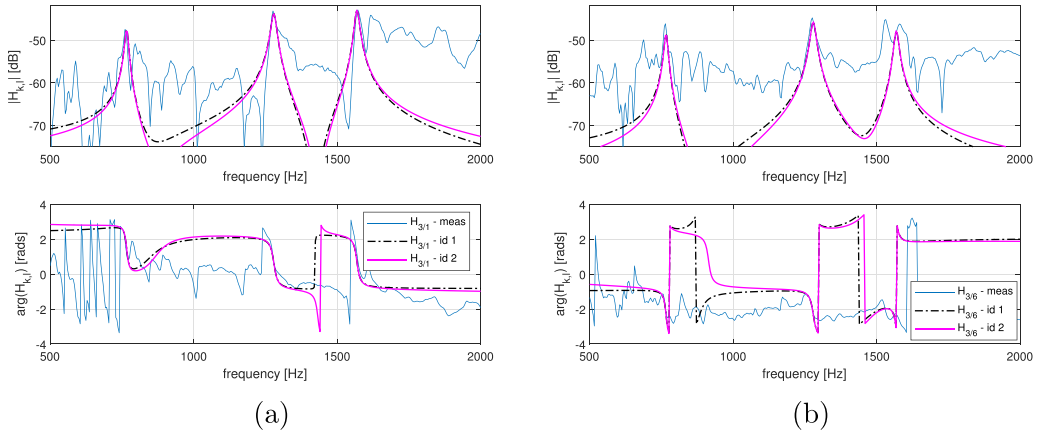

Figure 8. Identification : FRF's of PZT n°3 to actuation, (a) PZT 1 and (b) PZT 6, measurement, identification 1 with the formulation in (1), identification 2 with the proposed method in (7).

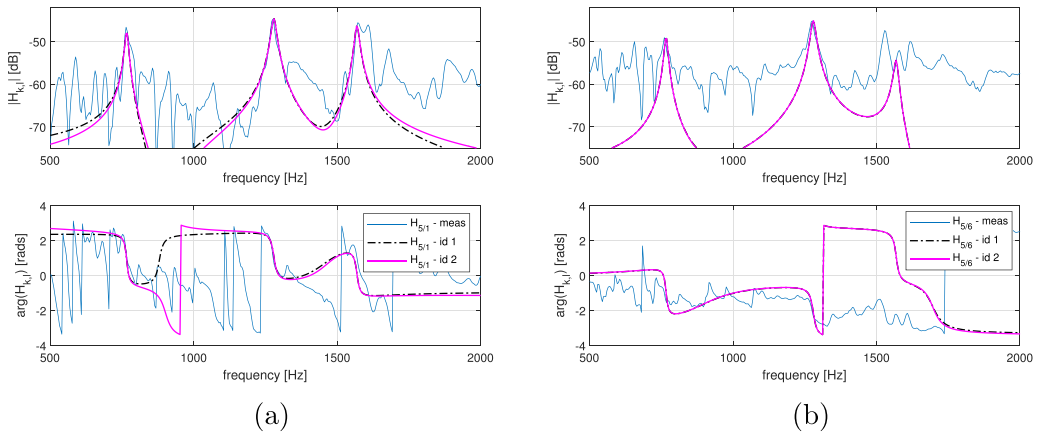

Figure 9. Identification : FRF's of PZT n°5 to actuation, (a) PZT 1 and (b) PZT 6, measurement, identification 1 with the formulation in (1), identification 2 with the proposed method in (7).

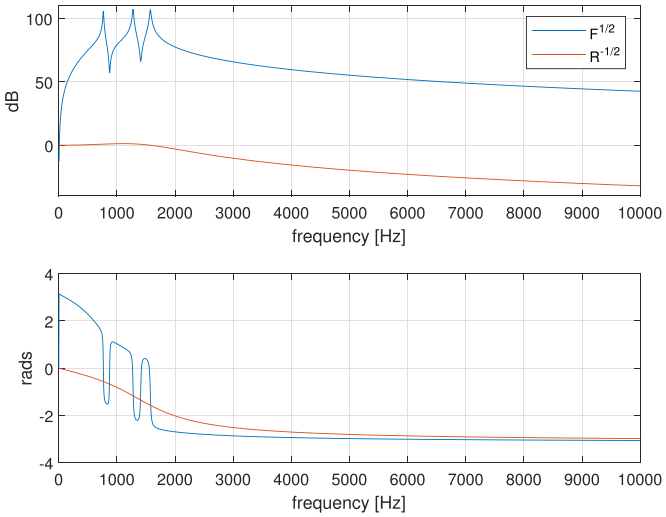

Figure 10. FRF of the designed pre- and post-filters $Q^{1/2}$ and $R^{-1/2}$.

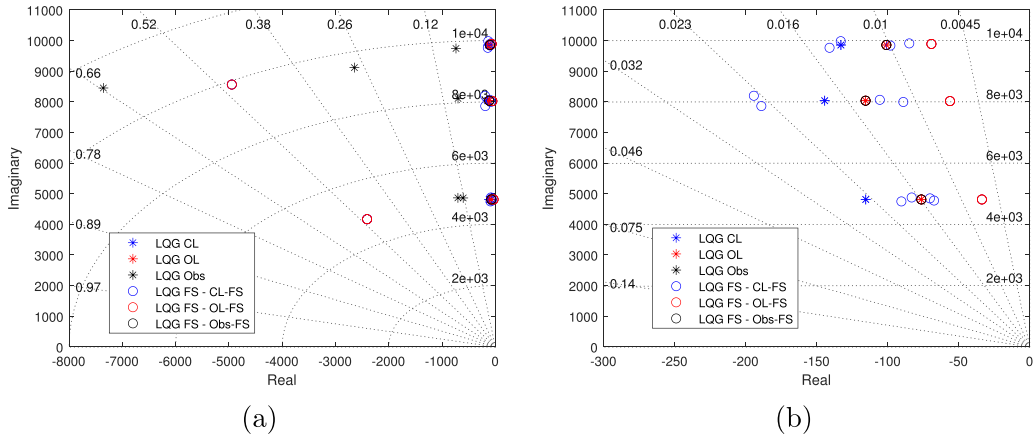

Figure 11. Poles locations: controlled system, uncontrolled system and observer for both control methods LQG and frequency shaped LQG, (a) global view and (b) zoom close to imaginary axis.

the weight matrices Q_0 and R_0 of the LQR associated LQR problem (A', B', Q_0, R_0) are:

$$Q_0 = 2 \times 10^4 \ \times I_{2\ nN_a}, \quad R_0 = I_{N_a} \tag{23}$$

where the gains are obtained for both controllers such that stability and sufficient robustness are maintained during the experiment with the same order of magnitude for the control voltages. In both cases, the Kalman observer is computed considering the following covariance matrices for process noise and measurement noise respectively: $V_d = I_{2\ nN_a}$ and $V_n = I_{N_s}$.

Finally the theoretical poles of the uncontrolled system and the controlled system with LQG control or LQG frequency-shaped control together with the observer poles are displayed in figure 11.

4.4. Experimental control results

Similarly to the identification process, a white noise signal of maximum amplitude 3 V and sampling frequency 20 kHz is applied to PZT 4 such as in figure 4.

The major results are presented in figure 12 which shows the power spectral densities of the PZT sensors 2, 3, and 5 with and without control. Firstly, one can notice that the amplitudes of the 3 target modes: 770, 1282, and 1576 Hz are significantly reduced. From -8 dB on the 3rd mode for PZT 5 to -20 dB on the 1st mode for PZT 3. Such control performance is very interesting regarding the drastic simplifications made during the identification process and the complexity of the real modal response of the structure.

However, such attenuation level presents also its drawbacks like the spillover phenomenon. Thus, the vibration amplitude can possibly increase at frequencies around the controlled modes due to the simplifications done in the

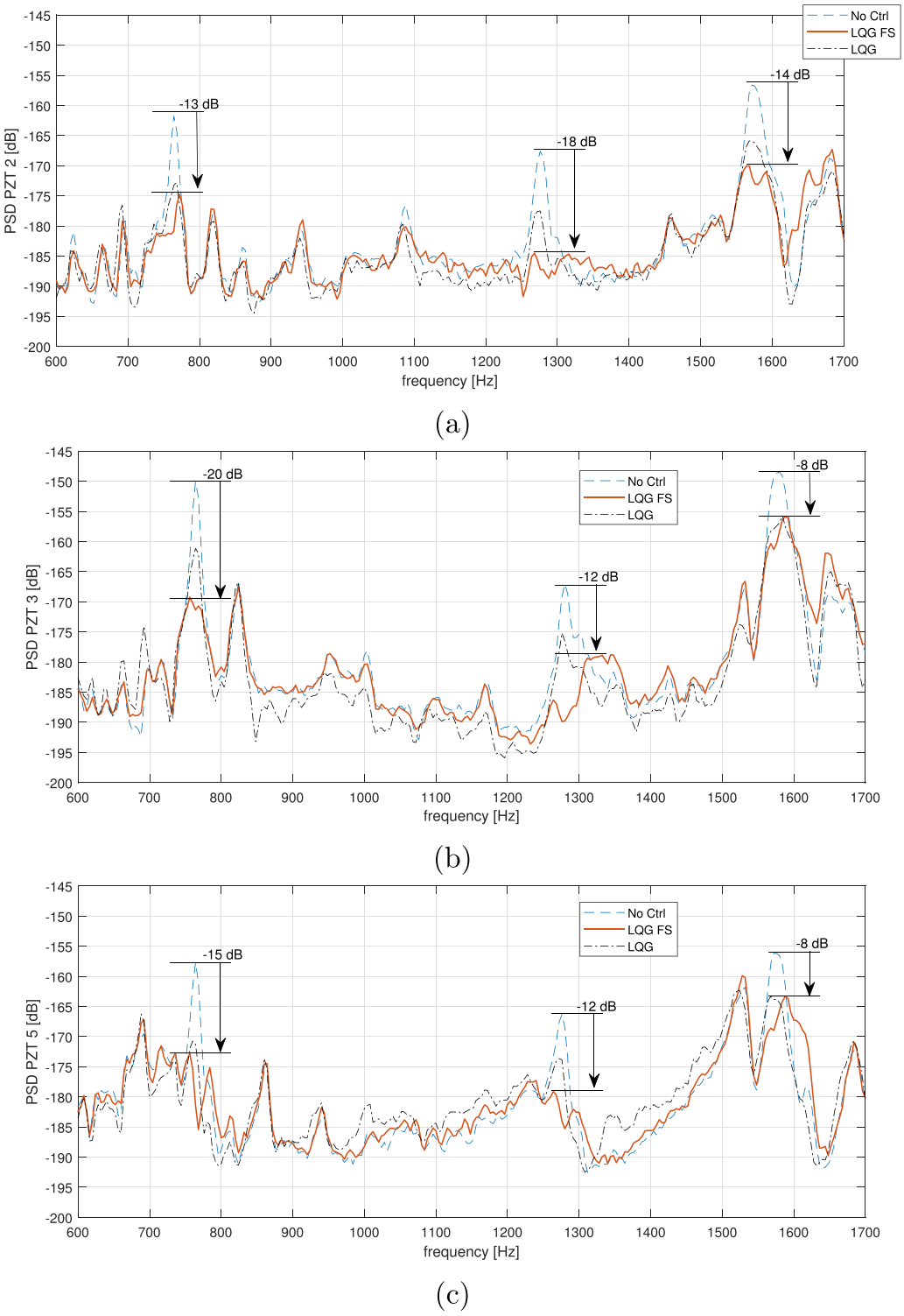

Figure 12. Power spectral density of the PZT sensors (a) PZT 2, (b) PZT 3, (c) PZT 5 without control, with LQG control and frequency-shaped LQG control.

identification process. The phase correction with the coefficients $a_i^{k,l}$ and $b_i^{k,l}$ is indeed only valid on a narrow bandwidth around the considered mode frequencies, causing the aforementioned performance degradation especially visible above the 3rd mode between 1600 and 1630 Hz on all PZT sensors.

For further comparison between the performances of both tested controllers, the figures 13 and 14 display the power spectral densities and time-domain extracts of the control signals from modal LQG control and frequency-shaped LQG control respectively. It is clearly observable, comparing the power spectral densities that the control energy is much

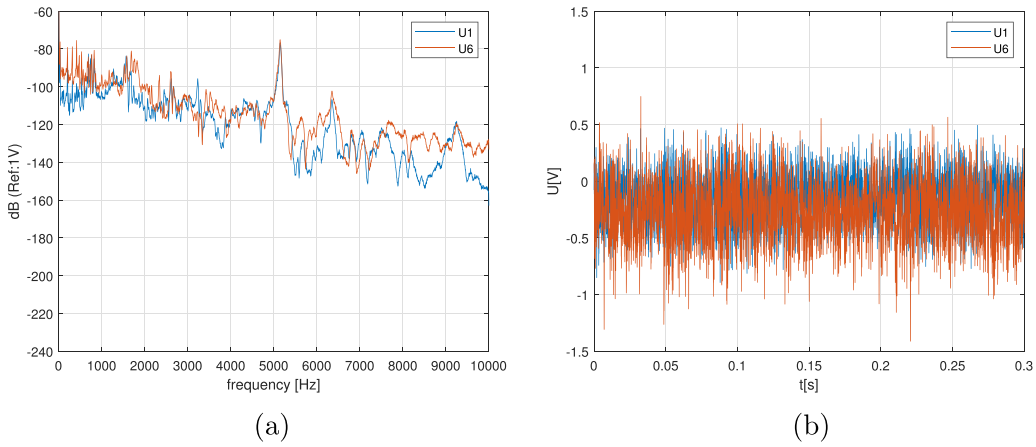

Figure 13. (a) Power spectral density of the control voltages for LQG and (b) time signals for 0.3 s.

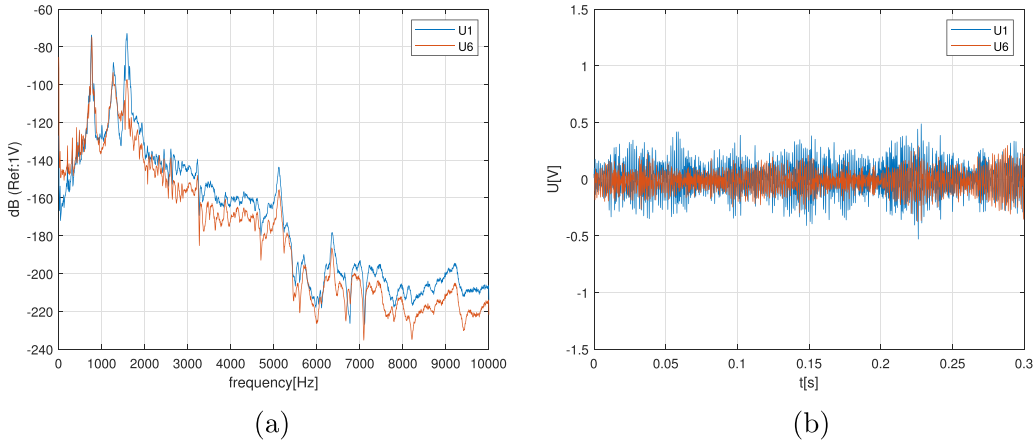

Figure 14. (a) Power spectral density of the control voltages for frequency-shaped LQG and (b) time signals for 0.3 s.

Table 2. RMS voltage values for excitation signal and both experimented controllers output signals.

	Voltage RMS value
Excitation—U_4	1.34
LQG—U_1	0.28
LQG—U_6	0.37
LQG-FS—U_1	0.13
LQG-FS—U_6	0.09

more focused on the targeted modes for frequency-shaped LQG.

Furthermore, the control signal maximum amplitudes are significantly reduced (see figures 13(b) and 14(b)) with a better attenuation level, as it can be observed in figure 12. Thus, table 2 displays the voltage RMS values for the excitation signal applied to the PZT 4 and the control signals applied to PZT actuators 1 and 6 by both tested controllers. Since PZT transducers used as actuators can support only a limited voltage input and present low authority under 500 Hz, frequency-shaped LQG control allows increasing the control gains while reducing non-necessary frequency components in the control signal.

We thank the referee for noticing maybe an unclear comment on the results. In this part of the manuscript, we are commenting the figures 13 and 14 and highlighting the amplitude reduction of the control signal especially visible in the time domain (figures 13(b) and 14(b)). The reference to the attenuation level on the modes is on the figure 12.

5. Conclusion

An experimental modal identification method has been proposed, oriented toward a multi-sensors, multi-actuators, and multi-controlled modes general approach. This global formulation allowed to bypass the usual difficulties of identifying the coupling coefficients in electromechanical systems. The novelty of the method mainly relied on replacing time delays in the real-time closed-loop with linear functions in the Laplace domain for phase correction at the frequencies of the modes. The final controller was based on the frequency-shaped linear quadratic method, using pre- and post- filters to focus the control energy onto the targeted modes. Finally, the controller was successfully applied to a representative composite smart structure where a network of transducers was fully integrated between the fiber layers with the complex frequency

behavior and electromechanical coupling that this entails. The experimental results in terms of multi-modal vibration control confirmed the efficacy of the proposed modal identification/control method which could now be applied to a wide range of dynamical structures with even larger transducer networks.

Data availability statement

The data that support the findings of this study are available upon reasonable request from the authors.

Acknowledgment

The authors would like to thank Institut Carnot for supporting the project and providing the funding for this research.

ORCID iDs

Jonathan Rodriguez https://orcid.org/0000-0001-8872-8968
Manuel Collet https://orcid.org/0000-0003-2049-0644
Simon Chesné https://orcid.org/0000-0003-1306-7231

References

[1] Tuloup C *et al* 2019 On the use of in-situ piezoelectric sensors for the manufacturing and structural health monitoring of polymer-matrix composites: a literature review *Compos. Struct.* **215** 127–49
[2] Shivashankar l and Gopalakrishnan P 2020 Review on the use of piezoelectric materials for active vibration noise and flow control *Smart Mater. Struct.* **29** 053001
[3] Safaei M, Sodano H A and Anton S R 2019 A review of energy harvesting using piezoelectric materials: state-of-the-art a decade later (2008–2018) *Smart Mater. Struct.* **28** 113001
[4] Khot S *et al* 2012 Active vibration control of cantilever beam by using PID based output feedback controller *J. Vib. Control* **18** 366–72
[5] Tairidis G K 2019 Vibration control of smart composite structures using shunted piezoelectric systems and neuro-fuzzy techniques *J. Vib. Control* **25** 2397–408
[6] Varadarajan S, Chandrashekhara K and Agarwal S 2000 LQG/LTR-based robust control of composite beams with piezoelectric devices *J. Vib. Control* **6** 607–30
[7] Wang S Y, Quek S T and Ang K K 2001 Vibration control of smart piezoelectric composite plates *Smart Mater. Struct.* **10** 637
[8] Jovanović M M *et al* 2013 Experimental studies on active vibration control of a smart composite beam using a PID controller *Smart Mater. Struct.* **22** 115038
[9] Malgaca L and Uyar M 2019 Hybrid vibration control of a flexible composite box cross-sectional manipulator with piezoelectric actuators *Composites* B **176** 107278
[10] Sohn J W, Choi S-B and Lee C-H 2009 Active vibration control of smart hull structure using piezoelectric composite actuators *Smart Mater. Struct.* **18** 074004
[11] Gao L *et al* 2013 Active vibration control based on piezoelectric smart composite *Smart Mater. Struct.* **22** 125032
[12] Li F-M, Song Z-G and Chen Z-B 2012 Active vibration control of conical shells using piezoelectric materials *J. Vib. Control* **18** 2234–56
[13] Berardengo M *et al* 2021 Vibration control with piezoelectric elements: the indirect measurement of the modal capacitance and coupling factor *Mech. Syst. Signal Process.* **151** 107350
[14] Chomette B *et al* 2008 Semi-adaptive modal control of on-board electronic boards using an identification method *Smart Mater. Struct.* **17** 065019
[15] Deng F, Rémond D and Gaudiller L 2011 Self-adaptive modal control for time-varying structures *J. Sound Vib.* **330** 3301–15
[16] Qiu Z *et al* 2007 Optimal placement and active vibration control for piezoelectric smart flexible cantilever plate *J. Sound Vib.* **301** 521–43
[17] Qiu Z *et al* 2009 Active vibration control of a flexible beam using a non-collocated acceleration sensor and piezoelectric patch actuator *J. Sound Vib.* **326** 438–55
[18] Li S *et al* 2013 Composite multi-modal vibration control for a stiffened plate using non-collocated acceleration sensor and piezoelectric actuator *Smart Mater. Struct.* **23** 015006
[19] Qiu Z 2015 Experiments on vibration suppression for a piezoelectric flexible cantilever plate using nonlinear controllers *J. Vib. Control* **21** 300–19
[20] Young P and Jakeman A 1980 Refined instrumental variable methods of recursive time-series analysis Part III. Extensions *Int. J. Control* **31** 741–64
[21] Garnier H, Mensler M and Richard A 2003 Continuous-time model identification from sampled data: implementation issues and performance evaluation *Int. J. Control* **76** 1337–57
[22] Chesné S, Jean-Mistral C and Gaudiller L 2013 Experimental identification of smart material coupling effects in composite structures *Smart Mater. Struct.* **22** 075007
[23] Laub A J *et al* 1987 Computation of system balancing transformations and other applications of simultaneous diagonalization algorithms *IEEE Trans. Autom. Control* **AC–32** 115–22
[24] Duc G and Mammar S 1991 Frequency-shaped LQG/LTR design: application to the robust stabilization of an helicopter *IFAC Proc. Volumes* **24** 39–44